HHS Public Access

Author manuscript

Biotechnol Bioeng. Author manuscript; available in PMC 2015 September 04.

Published in final edited form as:

Biotechnol Bioeng. 2014 May ; 111(5): 1028–1037. doi:10.1002/bit.25153.

Controlled local presentation of matrix proteins in microparticle-laden cell aggregates

Abigail B. Bernard[1], **Rebeccah Z. Chapman**[1], and **Kristi S. Anseth**[1,2,*]

[1]Department of Chemical and Biological Engineering, University of Colorado, Boulder, CO, 80303, U.S.A

[2]Howard Hughes Medical Institute, University of Colorado, Boulder, CO, 80303, U.S.A

Abstract

Multi-cellular aggregates are found in healthy and diseased tissues, and while cell-cell contact is important for regulating many cell functions, cells also interact, to varying degrees, with extra-cellular matrix (ECM) proteins. Islets of Langerhans are one such example of cell aggregates in contact with ECM, both at the periphery of the cluster and dispersed throughout. While several studies have investigated the effect of reintroducing contact with ECM proteins on islet cell survival and function, the majority of these experiments only allow contact with the exterior cells. Thus, cell-culture platforms that enable the study of ECM-cell interactions throughout multi-cellular aggregates are of interest.

Here, local presentation of ECM proteins was achieved using hydrogel microwell arrays to incorporate protein-laden microparticles during formation of MIN6 β-cell aggregates. Varying the microparticle seeding density reproducibly controlled the number of microparticles incorporated within three-dimensional aggregates (i.e., total amount of protein). Further, a relatively uniform spatial distribution of laminin- and fibronectin-coated microparticles was achieved throughout the x-, y-, and z-directions. Multiple ECM proteins were presented to β-cells in concert by incorporating two distinct populations of microparticles throughout the aggregates. Finally, scaling the microwell device dimensions allowed for the formation of two different sized cell-particle aggregates, ~80 and 160 μm in diameter. While the total number of microparticles incorporated per aggregate varied with size, the fraction of the aggregate occupied by microparticles was affected only by the microparticle seeding density, indicating that uniform local concentrations of proteins can be preserved while changing the overall aggregate dimensions.

Keywords

3D aggregates; adhesive proteins; microwell array; MIN6 β-cells

Corresponding Author Contact Information: Kristi S. Anseth, Mailing Address: Department of Chemical and Biological Engineering, University of Colorado, 3415 Colorado Avenue, Boulder, CO 80303, kristi.anseth@colorado.edu, Telephone: 303-492-3147, Fax: 303-735-0095.

Introduction

In the body, cells within numerous tissue types exist in multicellular clusters and are exposed to a complex milieu of both soluble cues and insoluble matrix interactions. One example is the islets of Langerhans, which are multicellular aggregates consisting of α-, β-, δ-, and other hormone-producing cells that signal to one another in a coordinated way to regulate blood glucose levels (Seeley et al., 2000; Samols et al., 1986). Soluble cues, including nutrients, growth factors, and hormones, are often transported to interior cells residing in such aggregates via a network of blood vessels and capillaries that deliver these and many other molecules. Solid matrix interactions also provide important cues and can be accessible to interior cells within aggregates via basal lamina that surrounds the blood vessels and capillaries found throughout the cell clusters. Research has shown that cells within multicellular aggregates are affected by the presence of both soluble and insoluble cues, and when isolated from the body or grown *in vitro*, recapitulating some of these key interactions found in cellular aggregates can be of critical importance in maintaining their function (Carpenedo et al., 2009; Carpenedo et al., 2010; Mahoney and Saltzman, 2001; Ravindran et al., 2011; Schukur et al., 2013; Zhu et al., 2007).

One way to introduce and control local interactions between and to cells within aggregates is through the incorporation of microspheres during aggregate formation. Microspheres can immobilize either insoluble matrix cues or release soluble cues in a manner that allows control of their spatiotemporal presentation in multicellular aggregates. Release of soluble cues to aggregated cells has been shown to promote stem cell differentiation (Carpenedo et al., 2009, 2010) and influence neuronal tissue response (Mahoney and Saltzman, 2001). Anchorage-dependent molecules, such as extra-cellular matrix (ECM) proteins and biologically relevant peptides, can also be tethered to particle surfaces to locally present insoluble cues that are also crucial for *in vitro* regulation of cell behavior in multi-cellular structures. Immobilized biological moieties delivered to three-dimensional cell aggregates via non-degradable microspheres have been shown to cause differentiation of adult stem cells (Ravindran et al., 2011), promote more healthy proliferation profiles in liver cells (Zhu et al., 2007), increase bone-like tissue formation from secretions of stromal cells (Qiu et al., 2001), and support the *in vitro* culture of islet cells in an artificial pancreas (Silva and Mateus, 2009).

The *in vitro* culture of pancreatic islets of Langerhans might also benefit from the spatial introduction of insoluble matrix cues. By interactions with the basal lamina that envelopes the islet, as well as the double basement membrane that surrounds the walls of blood vessels within islets (Virtanen et al., 2008), cells throughout the islet are in contact with several insoluble ECM proteins, such as collagen types I and IV, laminin, and fibronectin (van Deijnen et al., 1992; Wang and Rosenberg, 1999). Previous research focused on the *in vitro* culture of islets has shown that re-introduction of certain ECM proteins significantly reduces global apoptosis and increases insulin production, even though, presumably, only the exterior cells of the islet are in contact with the matrix signals (Daoud et al., 2010; Nagata et al., 2001; Weber and Anseth, 2008). Further, modifying synthetic encapsulation materials with protein-derived peptides (e.g., IKVAV, IKLLI, RGDS, GLP-1) has shown similar

positive effects on islet viability and function (Duncanson and Sambanis, 2013, Lin and Anseth, 2009a; Weber et al., 2007).

While these approaches make strides towards demonstrating the potential importance of re-introducing cues found in the basal lamina during islet culture, little is known about how the distribution of these signals influences functional properties (i.e., controlling cell-matrix interactions throughout the aggregate). Since introducing ECM interactions throughout multicellular β-cell aggregates in a controlled fashion can be challenging, we developed a scheme using synthetic microspheres modified with either fibronectin or laminin by surface adsorption and then used a hydrogel microwell array (Bernard et al., 2012) to create microsphere-laden β-cell aggregates of defined sizes and particle contents. By varying the amount of particles incorporated within an aggregate, different concentrations of proteins can be introduced to cells locally. Additionally, multiple populations of microspheres, each coated with a different protein, can be incorporated within the same cluster to study the synergistic effects of various ratios of proteins on aggregate cell function.

Materials and Methods

Protein adsorption to microparticles

Spherical microparticles based on a melamine resin, 1 μm in diameter and fluorescently-labeled with either Rhodamine B or Nile Blue were purchased from Sigma, and matrix proteins were physically adsorbed to the surface via the manufacturer's instructions (details in Supplemental Methods). Total protein adsorbed to the microparticles was quantified using a microBCA assay (Pierce, Rockford, IL) (Table SI) by first desorbing from the particles using a surfactant, sodium dodecyl sulfate (SDS, Sigma, St. Louis, MO). Solutions of fibronectin and laminin in SDS were used to generate standard curves.

MIN6 cell culture

MIN6 cells (P26–P36) were kept in T75 flasks (Corning, Corning, NY) and supported with high glucose (4.5 g/L) Dulbecco's Modified Eagle Medium (DMEM, Gibco, Carlsbad, CA) supplemented with 10% fetal bovine serum (FBS, Gibco), 1% PenStrep (Gibco), 0.2% Fungizone (Gibco), 1 mM sodium pyruvate (Sigma) and 60 μM 2-mercaptoethanol (Sigma). Media was changed every 3–4 days and cells were split 1:3 weekly.

Microwell array and cell-particle aggregate formation

Microwell arrays were formed via a published protocol (Bernard et al., 2012) using a macromer solution containing poly(ethylene glycol) (PEG) synthesized as described previously (Lin and Anseth 2009b). A schematic of the microwell formation is shown in Figure 1A–C and details of microwell formation are presented in the Supplemental Methods. Cell culture wells were fabricated with a fixed depth of 100 μm and square cross-sections of either 100 μm × 100 μm (w100) or 200 μm × 200 μm (w200). Microwell arrays were sterilized by quick immersion in 70% ethanol, followed by swelling in sterile HBSS containing 1% Pen Strep and 0.2% Fungizone under a germicidal UV light for at least 1 hour.

MIN6 cells were removed from culture flasks and stained with 10 μM CellTracker Green CMFDA (Life Technologies, Carlsbad, CA) for visualization. Single cell suspensions of dyed MIN6 were first pre-incubated overnight on an orbital shaker (35 rpm) in polypropylene Eppendorf tubes (VWR) with an appropriate number of microparticles to achieve a particle-to-cell ratio of 1:5 (i.e., 1 microparticle for every 5 cells), 1:1, or 5:1. After pre-incubation, the cells and particles were seeded into the microwell devices by centrifugation at 1200 rpm for 150 s (Fig. 1D–F) as described previously (Bernard et al., 2012; Kloxin et al., 2012; Ruiz and Chen, 2008). Unseeded cells and microparticles were gently resuspended and the centrifugation seeding step was repeated. The well plates were placed on an orbital shaker at 37°C and 5% CO_2 for 2 hours and then cultured statically for 5 days to allow for aggregate formation as shown by previous studies (Bernard et al., 2012). After 5 days, the cell-microparticle aggregates were removed from the microwell device arrays by gentle rinsing with media and single cells and unincorporated microparticles were removed by separation via cell strainers (BD Falcon). This aggregation method produced cell-microparticle structures that were robust enough to maintain their size and cohesiveness through removal from the microwell arrays and further analysis. Vigorous pipetting and vortexing can disturb the cell-cell adhesiveness sufficiently enough to cause the break up of these clusters (data not shown). Aggregates from w100 and w200 microwells contained approximately 500 and 800 cells, respectively (Bernard et al., 2012).

Confocal microscopy and image analysis

Cell-microparticle aggregates were imaged on a Zeiss LSM 710 NLO (Carl Zeiss, Oberkochen, Germany) using λ=488 nm laser to visualize the cells (green), λ=541 nm laser to image the Rhodamine-labeled particles (red), and λ=633 nm laser to excite the Nile Blue-labeled particles (blue). Images were taken at 2 μm z increments and the images were compressed into 10 μm stacks (5 images per stack) for image analysis. A minimum of 30 cell-microparticle aggregates formed under each condition from at least 3 independent cell seeding events were analyzed. More details are provided in the Supplemental Methods.

Statistical analysis

Statistical significance was determined using a student's t-test with Welch's correction for unequal variances and a 95% confidence interval or ANOVA with Tukey's test, as indicated. A p-value < 0.05 is denoted by an asterisk (*) in the figures.

Results and Discussion

Creating cell-microparticle aggregates

Cell-microparticle aggregates of defined and uniform sizes were created using centrifugation and a hydrogel microwell device array (Bernard et al., 2012; Kloxin et al., 2012; Ruiz and Chen, 2008) to template their formation. A simplified schematic of the cell-microparticle aggregation process is shown in Figure 1. Protein-coated microparticles were first incubated with cells overnight (Fig. 1D) to facilitate cell-particle interactions and attachment. This pre-incubation was performed to achieve a more efficient and even distribution of microparticles throughout the cell aggregates, as the independent cells and microparticles (i.e., without any pre-incubation) can have different settling times during seeding in the devices (Fig. S3).

After this incubation period, cells and microparticles were seeded into hydrogel microwell arrays (Fig. 1E) using centrifugation and orbital shaking, as previously described (Bernard et al., 2012). After five days in static culture, the cell-microparticle aggregates were removed from the microwell arrays (Fig. 1F) and imaged to assess microparticle incorporation within the aggregates. Removing the cell-microparticle aggregates from the microwell arrays was crucial for proper assessment of microparticle incorporation to ensure that loose microparticles, which were seeded into the microwell arrays but not incorporated into the cell-particle aggregates, were removed prior to analysis.

Analyzing the spatial distribution of microparticles within 3D cell aggregates

To assess the spatial distribution of the ECM-coated microparticles within the 3D β-cell aggregates, image analysis was performed throughout the z-direction of confocal images, taken at 2 μm intervals. An example of this analysis is shown in Figure 2 and Figures S1 and S2. First, all individual z-planes of the cell-microparticle aggregate were compressed into a maximum z-projection of the entire aggregate (Fig. 2A) to determine the area of the image to analyze, that is, the x-y location (in pixels) of the image occupied by each aggregate. Next, the original, single plane images were stacked into smaller projections representing 10 μm sections of the aggregate (Fig. 2B–E). Each 10 μm stack was then analyzed to assess the number of green pixels (representative of MIN6 cells stained with a cytoplasmic dye, Fig. 2F–I) and red pixels (illustrating microparticle presence, Fig. 2J–M) contained within the mask of that particular aggregate. These data were then used to determine both the total number of incorporated microparticles, as well as the distribution of these microparticles throughout the 3D aggregate. On average, each laminin-coated resin particle appeared as 11 square pixels in the compressed confocal image (determined by imaging and measuring single particles, data not shown). The number of red pixels in each stack was converted to an approximate number of microparticles in that layer by dividing by the average number of pixels per particle. The number of microparticles was summed from each stack to give an estimate of the total microparticles within an aggregate. Finally, the percentage of the cross-sectional area of an aggregate in each 10 μm stack that was occupied by microparticles was calculated to assess the spatial distribution of microparticles throughout the cell aggregates. The particle cross-sectional area was defined as the percentage of pixels within the aggregate mask of a stacked image that contained particles (red pixels) compared to the total number of pixels (red and green).

Cell-microparticle seeding ratio influences particle incorporation

MIN6 β-cells and laminin-coated resin microparticles were pre-incubated at various concentrations of microparticles to vary the particle incorporation, and therefore, the amount of protein delivered to the cells within the cell-microparticle aggregates. Cells incubated with three ratios of laminin-coated microparticles – one particle for every five cells (1:5), one particle for every cell (1:1), and five particles for every cell (5:1) – were seeded into hydrogel microwell arrays. After five days of culture, the cell-microparticle aggregates were removed from the arrays and imaged. These results are presented in Figure 3. Total z-projections of confocal images (100 μm deep) taken of MIN6 cells (green) aggregated with varying amounts of laminin-coated resin particles (red) are shown in Figure 3A–C. Varying the seeding ratio of particles to cells did not affect the ability of MIN6 cells to aggregate in

the hydrogel microwell arrays over the concentrations studied. Relatively uniform cell cluster size and microparticle incorporation were observed in the x-, y-, and z-dimensions, regardless of particle seeding density, and a noticeable increase in the number of particles within the cell aggregates was observed when the initial particle density was increased.

The effect of initial microparticle seeding density on the spatial distribution and total microparticle incorporation within these β-cell aggregates was quantified using image analysis via MATLAB (as presented in Fig. 2). The average number of incorporated microparticles after varying the particle incorporation density and the distribution of these particles throughout the cell aggregates are presented in Figure 3D. While the number of microparticles incorporated into the β-cell aggregates did not scale directly with incubation conditions, there was a significant increase in the number of incorporated microparticles when the seeding ratio was increased from 1:5 (80 ± 20 microparticles per aggregate) to 1:1 (140 ± 30 microparticles per aggregate) and then increased again to 5:1 (360 ± 50 microparticles incorporated). This trend indicates that the spatial presentation of total protein throughout the multi-cellular β-cell aggregates can be varied from 0.90 pg (1:5) to approximately 4.3 pg of laminin (5:1) using this method (Table I). In general, these aggregates were ellipsoidal in shape with a minor axis of 80 μm and a major axis of 160 μm, containing ~800 cells (Bernard et al., 2012).

To quantify the spatial distribution of microparticles within the aggregates, the fraction of the cross-sectional area occupied by microparticles was also analyzed (Fig. 3E). These data demonstrate a relatively uniform incorporation of microparticles throughout the cell aggregates, indicating good dispersion of the protein to many cells within the aggregates. Additionally, although the microparticles are denser than the cells, pre-incubation of cells with the particles prior to seeding helped to promote a more even distribution throughout the aggregate. Without this pre-incubation, large numbers of particles settle to the bottom of device during aggregation, resulting in a non-uniform distribution of protein (Supplemental Information, Fig. S3).

Controlling and manipulating the distribution of protein-coated microparticles within cell aggregates should provide a useful tool to better understand how local presentation of ECM ligands influences the function of β-cell aggregates, perhaps more closely mimicking native islet architecture in which cells throughout islets are in contact with basement membrane proteins that comprise the capillary walls. Islets cultured on protein-coated surfaces (Daoud et al., 2010, Nagata et al., 2001; Wang and Rosenberg, 1999) and encapsulated within protein-containing materials (Oberg-Welsh, 2001; Na et al., 2001; Weber and Anseth 2008) show increased viability and insulin secretion where, presumably, only a small fraction of the cells are in contact with the matrix molecules. By incorporating proteins throughout cellular aggregates, a higher percentage of cells could have access to these cues, which may influence their functional response dynamics. Moreover, investigating protein presentation in this way may overcome inherent biasing of studies towards smaller aggregates that contain a higher fraction of periphery cells, as traditional methods only provide contact of exterior cells with the ECM ligands.

Simultaneous, local presentation of two different ECM proteins throughout cell aggregates

To develop a platform in which multiple, insoluble, tethered cues may be presented in concert throughout multi-cellular β-cell aggregates, we first created two populations of protein-laden microparticles: microparticles labeled with Rhodamine-B and coated with laminin (LN) and microparticles labeled with Nile Blue and coated with fibronectin (FN). We then studied how varying ratio of these microparticles influenced their incorporation, and thus, the amount of each protein presented to the cells. Specifically, the ratio of the two particles was varied from 3:1 to 1:1 to 1:3, FN:LN, respectively, while keeping the total number of particles seeded in each device, five particles for every cell, the same. These results are presented in Figure 4.

Using this method, both LN- and FN-modified resin microparticles were incorporated into β-cell aggregates. Confocal images of the cell-microparticle aggregates showed good dispersion of both types of particles throughout the aggregates (Fig. 4A–C), indicating a relatively uniform seeding of the particles in the x-, y-, and z-directions. This distribution was quantified in a manner similar to the analysis performed to produce Figure 3E, and the results are presented in the Supplemental Information, Figure S4. Interestingly, the ratio of the two populations of particles, as well as the total number of particles incorporated within the aggregates, did not scale with the initial microparticle seeding conditions (Fig. 4D–E).

To better understand these results, we observed that the number of Nile Blue-labeled resin particles coated with fibronectin did scale roughly, as expected, with seeding conditions (Fig. 4E, Table I). For example, the FN-modified particle content decreased by approximately one-third when the number of FN microparticles seeded with β-cells was reduced by one-third. However, the number of Rhodamine B-labeled, LN-coated microparticles incorporated within the β-cell aggregates did not change significantly when the total number of LN-coated particles pre-incubated with the cells was doubled (Fig. 4D). Instead, a slight but significant increase was observed when incorporating the laminin-coated microparticles at the highest seeding ratio (five microparticles for every cell, 75% LN-coated and 25% FN-coated).

Additionally, the total number of microparticles (five particles per cell) seeded with the β-cells was held constant for all ratios of LN:FN microparticle seeding densities; however, the total number of measured particles incorporated within the cell-microparticle aggregates decreased with seeding condition (Fig. 4D). We hypothesize that this difference was due to the inefficient incorporation of LN-coated microparticles relative to the FN-coated microparticles, perhaps due to differences in the integrin-binding affinity or integrin presentation on MIN6 β-cells. To date, limited information is available related to specific integrin presentation of MIN6 β-cells, but they have been shown to adhere to the cell adhesion peptide sequence Arginine-Glycine-Aspartate (RGD), the hallmark sequence found in fibronectin and also present in many other ECM proteins, including some forms of laminin (Na et al., 2001; Park et al., 2005; Yamada, 1991). Additionally, primary β-cells from various species have been shown to express cell surface receptors for fibronectin and laminin. Specifically, cell surface receptors $\alpha_v\beta_3$, $\alpha_3\beta_1$, and $\alpha_5\beta_1$ which have affinity for both fibronectin and laminin, as well as $\alpha_v\beta_1$ which binds fibronectin, and $\alpha_1\beta_1$, $\alpha_6\beta_1$, and the 67-kDa laminin receptor, which bind laminin, have all been identified on β-cells (Bosco

et al., 2000; Jiang et al., 2002; Kaido et al., 2004; Ris et al., 2002; Virtanen et al., 2008; Weber et al., 2008; Yamada, 1991). While β-cells are known to adhere to both laminin and fibronectin *in vitro*, these cells show increased adhesion to fibronectin over laminin, adhesion being the dominant interaction of β-cells with fibronectin and laminin showing greater effects in pseudo-islet formation and insulin secretion regulation (Daoud et al., 2010; Maillard et al., 2009). This reported disparity in adhesion to these two ECM proteins may influence microparticle association during the pre-incubation steps and ultimately microparticle incorporation. Differences in cell affinity for various ECM ligands should be taken into consideration when using this method to simultaneously present multiple cues within cell aggregates. Of further note, the FN-coated particles also appear to cluster together and form larger particle agglomerates after protein adsorption (Fig. S6), and during pre-incubation with the MIN6 cells, which may, in part, explain an enhanced incorporation of these particles during aggregate formation.

In general, this cell-microparticle aggregate formation technique could be translated to study the incorporation of a variety of insoluble molecules with varying affinities for β-cells and which bind different integrins. For example, collagen type IV also constitutes a large percentage of the basement membrane proteins found in islets, binds cell surface receptors $\alpha_1\beta_1$ and $\alpha_v\beta_1$ on β-cells, and has been implicated in cell adhesion as well as insulin secretion (Daoud et al., 2010; Weber et al., 2008). Studying different ECM molecules could also allow the investigation of whether binding of different integrins and the affinity of different molecules for β-cells affects microparticle incorporation as appears true with laminin- and fibronectin-coated microparticles. Biologically, it would also be relevant to study the effect of the incorporation of protein-coated microparticles on β-cell function, specifically, insulin secretion in response to glucose. Additionally, synergistic effects of incorporating multiple ECM cues simultaneously might be investigated by incorporating multiple populations of microparticles coated with various ligands.

Manipulating aggregate size changes the number of incorporated microparticles, but not the relative particle density

Different sized β-cell-microparticle aggregates were formed by seeding microparticles and cells (at a ratio of 1:5) in hydrogel microwell device arrays containing wells of two different cross-sectional areas and volumes: 100 μm × 100 μm × 100 μm (w100) microwells and 200 μm × 200 μm × 100 μm (w200) microwells. After culture, removal, and imaging, the total number of incorporated LN-coated microparticles per aggregate, as well as the spatial distribution of the microparticles within the aggregates, were analyzed and the results are summarized in Figure 5. Significantly more microparticles were incorporated into the w200 aggregates (160 ± 30) compared to the w100 aggregates (60 ± 10) ($p<0.01$) (Fig. 5C).

We next determined the fraction of the aggregates comprised of microparticles to ascertain whether microwell size affected microparticle seeding. Promisingly, the percentage of the aggregate comprised of microparticles was relatively constant at 1.3% ± 0.3% for w100 aggregates and 1.9% ± 0.3% for w200 aggregates (Fig. 5D), indicating that the ratio of cells to particles can be controlled while varying the aggregate size. Additionally, the cross-sectional area of the aggregate composed of microparticles did not change with aggregate

size (Fig. S5) demonstrating relatively uniform presentation of ECM proteins throughout the multi-cellular aggregates, regardless of aggregate size. Therefore, this method shows promise for creating cell-microparticle aggregates of different sizes that could be used to study synergistic effects of aggregate size, or degree of cell coupling, and local presentation of ECM ligands throughout three-dimensional aggregates. Natively, islets exist as a heterogeneous distribution of sizes with rodent islets typically measuring from 50 μm to 300 μm in diameter (Lehmann et al., 2007; Takei et al., 1994). Islet size has been implicated in cell survival and function post-isolation (Lehmann et al., 2007; MacGregor et al., 2006); and the introduction of matrix molecules further impact islet cell function (Nagata et al., 2001; Wang and Rosenberg, 1999; Weber and Anseth, 2008). This cell-microparticle formation method could fill a critical void in the ability to simultaneously investigate the effect of cell aggregate size and local protein presentation.

The presented technique to form 3D, multicellular, cell-microparticle aggregates also has the potential to be used in a fundamental way to study islet cell biology. In addition to the examples shown above, large numbers of microparticles, or microparticles of larger dimensions, could be systematically introduced to mimic defects within pancreatic islets, areas in which cell-cell communication is disrupted. Cells within an islet coordinate through electrical pulses and ion flux through gap junctions of connected cells to regulate dynamic and pulsatile insulin release (Benninger et al, 2008, 2011; Head et al., 2012). A percolation theory-based model has been suggested to explain the minimum amount of cell coupling necessary for an entire islet to be effectively coordinated (Benninger et al., 2008). This model could be further investigated by the controlled introduction of void spaces, through the incorporation of microparticles, to achieve aggregates of β-cells above, at, and below the critical connectivity density determined via percolation theory. Subsequent analysis of the cell-cell communication in these clusters could further validate the model and garner additional understanding of the way β-cells communicate and overcome defects in cell coupling.

Alternatively, this technique could be used to further elucidate which aspects of cell-cell contact are most critical for proper β-cell function. Microparticles can be functionalized with any number of biological moieties that can successfully mimic cell-cell contact such as EphA and Ephrin-A (Konstantinova et al., 2007; Lin and Anseth 2011), E-cadherin (Calabrese et al., 2004; Jaques et al., 2008; Rogers et al., 2007), or Connexin-36 (Benninger et al, 2011; Carvalho et al., 2012; Head et al., 2012; Jaques et al., 2008). Lin and Anseth (2011) used a combination of EphA, ephrinA, and RGDS to promote β-cell survival at low seeding densities in synthetic hydrogels in the absence of direct cell-cell contact. Additionally, when preventing cell-cell interactions via E-cadherin proteins, Rogers *et al.* documented a significant decrease in insulin secretion from β-cells (Rogers et al., 2007). Similarly, when the gap junction forming protein connexin-36 is knocked-down in β-cells within islet cell clusters, Head *et al.* (2012) found a resulting decrease in islet cell coordination and insulin release. Using these types of molecules alone or in concert, along with changing the amount of cell-cell contact allowed through the introduction of microparticles as void spaces, could enable the study of the effect of specific cell-cell interaction proteins on β-cell survival and insulin release.

Conclusions

Cell-microparticle aggregates were formed with MIN6 β-cells and protein-laden resin microparticles using hydrogel microwell arrays. The total amount of incorporated microparticles, and therefore, the amount of adsorbed ECM protein presented to cells, was controlled by varying cell-microparticle seeding conditions. Additionally, multiple matrix cues were presented in concert within β-cell aggregates by the incorporation of two distinct populations of microparticles containing laminin and fibronectin. Whether a singular ECM molecule was presented or two different moieties were incorporated simultaneously, the distribution of microparticles throughout the cell aggregate was relatively uniform. Changing aggregate size resulted in a change in total microparticle incorporation, but the fraction of the aggregate occupied by microparticles was unaffected by aggregate size, only by microparticle seeding conditions. Collectively, these results demonstrate a versatile technique to integrate a range of microparticle concentrations and compositions into cellular aggregates of physiologically-relevant sizes. In addition to the utility shown in this work, this cell-microparticle formation platform has the potential to illuminate many other areas of islet cell biology and the investigation of phenomena affected aggregated cells of a variety of cell types.

Supplementary Material

Refer to Web version on PubMed Central for supplementary material.

Acknowledgments

The authors wish to gratefully acknowledge financial support from the National Institutes of Health (NIH grant R01DK076084) and the Howard Hughes Medical Institute. We would also like to acknowledge the contributions of Dr. Melissa Pope for help with image processing and Danielle Metzner and Kelly Shekiro for experimental assistance.

References

Benninger RKP, Head WS, Zhang M, Satin LS, Piston DW. Gap junctions and other mechanisms of cell-cell communication regulate basal insulin secretion in the pancreatic islet. Journal of Physiology-London. 2011; 589(22):5453–5466.

Benninger RKP, Zhang M, Head WS, Satin LS, Piston DW. Gap Junction Coupling and Calcium Waves in the Pancreatic Islet. Biophysical Journal. 2008; 95(11):5048–5061. [PubMed: 18805925]

Bernard AB, Lin CC, Anseth KS. A Microwell Cell Culture Platform for the Aggregation of Pancreatic beta-Cells. Tissue Engineering Part C-Methods. 2012; 18(8):583–592. [PubMed: 22320435]

Bosco D, Meda P, Halban PA, Rouiller DG. Importance of cell-matrix interactions in rat islet beta-cell secretion in vitro - Role of alpha 6 beta 1 integrin. Diabetes. 2000; 49(2):233–243. [PubMed: 10868940]

Calabrese A, Caton D, Meda P. Differentiating the effects of Cx36 and E-cadherin for proper insulin secretion of MIN6 cells. Experimental Cell Research. 2004; 294(2):379–391. [PubMed: 15023528]

Carpenedo RL, Bratt-Leal AM, Marklein RA, Seaman SA, Bowen NJ, McDonald JF, McDevitt TC. Homogeneous and organized differentiation within embryoid bodies induced by microsphere-mediated delivery of small molecules. Biomaterials. 2009; 30(13):2507–2515. [PubMed: 19162317]

Carpenedo RL, Seaman SA, McDevitt TC. Microsphere size effects on embryoid body incorporation and embryonic stem cell differentiation. Journal of Biomedical Materials Research Part A. 2010; 94A(2):466–475. [PubMed: 20213812]

Carvalho CPF, Oliveira RB, Britan A, Santos-Silva JC, Boschero AC, Meda P, Collares-Buzato CB. Impaired beta-cell-beta-cell coupling mediated by Cx36 gap junctions in prediabetic mice. American Journal of Physiology-Endocrinology and Metabolism. 2012; 303(1):E144–E151. [PubMed: 22569071]

Daoud J, Petropavlovskaia M, Rosenberg L, Tabrizian M. The effect of extracellular matrix components on the preservation of human islet function in vitro. Biomaterials. 2010; 31(7):1676–1682. [PubMed: 20015544]

Duncanson S, Sambanis A. Dual factor delivery of CXCL12 and Exendin-4 for improved survival and function of encapsulated beta cells under hypoxic conditions. Biotechnology and Bioengineering. 2013; 110:2292–2300. [PubMed: 23436382]

Head WS, Orseth ML, Nunemaker CS, Satin LS, Piston DW, Benninger RKP. Connexin-36 Gap Junctions Regulate In Vivo First- and Second-Phase Insulin Secretion Dynamics and Glucose Tolerance in the Conscious Mouse. Diabetes. 2012; 61(7):1700–1707. [PubMed: 22511206]

Jaques F, Jousset H, Tomas A, Prost AL, Wollheim CB, Irminger JC, Demaurex N, Halban PA. Dual effect of cell-cell contact disruption on cytosolic calcium and insulin secretion. Endocrinology. 2008; 149(5):2494–2505. [PubMed: 18218692]

Jiang FX, Naselli G, Harrison LC. Distinct distribution of laminin and its integrin receptors in the pancreas. Journal of Histochemistry & Cytochemistry. 2002; 50(12):1625–1632. [PubMed: 12486084]

Kaido T, Perez B, Yebra M, Hill J, Cirulli V, Hayek A, Montgomery AM. alpha(v)-Integrin utilization in human beta-cell adhesion, spreading, and motility. Journal of Biological Chemistry. 2004; 279(17):17731–17737. [PubMed: 14766759]

Kloxin AM, Lewis KJR, DeForest CA, Seedorf G, Tibbitt MW, Balasubramaniam V, Anseth KS. Responsive culture platform to examine the influence of microenvironmental geometry on cell function in 3D. Integrative Biology. 2012; 4(12):1540–1549. [PubMed: 23138879]

Konstantinova I, Nikolova G, Ohara-Imaizumi M, Meda P, Kucera T, Zarbalis K, Wurst W, Nagamatsu S, Lammert E. EphA-ephrin-A-mediated beta cell communication regulates insulin secretion from pancreatic islets. Cell. 2007; 129(2):359–370. [PubMed: 17448994]

Lehmann R, Zuellig RA, Kugelmeier P, Baenninger PB, Moritz W, Perren A, Clavien PA, Weber M, Spinas GA. Superiority of small islets in human islet transplantation. Diabetes. 2007; 56(3):594–603. [PubMed: 17327426]

Lin CC, Anseth KS. Controlling Affinity Binding with Peptide-Functionalized Poly(ethylene glycol) Hydrogels. Advanced Functional Materials. 2009a; 19(14):2325–2331. [PubMed: 20148198]

Lin CC, Anseth KS. Glucagon-Like Peptide-1 Functionalized PEG Hydrogels Promote Survival and Function of Encapsulated Pancreatic beta-Cells. Biomacromolecules. 2009b; 10(9):2460–2467. [PubMed: 19586041]

Lin CC, Anseth KS. Cell-cell communication mimicry with poly(ethylene glycol) hydrogels for enhancing beta-cell function. Proceedings of the National Academy of Sciences of the United States of America. 2011; 108(16):6380–6385. [PubMed: 21464290]

MacGregor RR, Williams SJ, Tong PY, Kover K, Moore WV, Stehno-Bittel L. Small rat islets are superior to large islets in in vitro function and in transplantation outcomes. American Journal of Physiology-Endocrinology and Metabolism. 2006; 290(5):E771–E779. [PubMed: 16303846]

Mahoney MJ, Saltzman WM. Transplantation of brain cells assembled around a programmable synthetic microenvironment. Nature Biotechnology. 2001; 19(10):934–939.

Maillard E, Sencier MC, Langlois A, Bietiger W, Krafft MP, Pinget M, Sigrist S. Extracellular matrix proteins involved in pseudoislets formation. Islets. 2009; 1(3):232–241. [PubMed: 21099277]

Na K, Choi HK, Akaike T, Park KH. Conjugation of Arg-Gly-Asp (RGD) sequence in copolymer bearing sugar moiety for insulinoma cell line (MIN6) culture. Bioscience Biotechnology and Biochemistry. 2001; 65(6):1284–1289.

Nagata N, Gu Y, Hori H, Balamurugan AN, Touma M, Kawakami Y, Wang WJ, Baba TT, Satake A, Nozawa M, et al. Evaluation of insulin secretion of isolated rat islets cultured in extracellular matrix. Cell Transplantation. 2001; 10(4–5):447–451. [PubMed: 11549070]

Oberg-Welsh C. Long-term culture in Matrigel enhances the insulin secretion of fetal porcine islet-like cell clusters in vitro. Pancreas. 2001; 22(2):157–163. [PubMed: 11249070]

Park KH, Na K, Jung SY, Kim SW, Cha KY, Chung HM. Insulinoma cell line (MIN6) adhesion and spreading mediated by Arg-Gly-Asp (RGD) sequence conjugated in thermo-reversible gel. Journal of Bioscience and Bioengineering. 2005; 99(6):598–602. [PubMed: 16233837]

Qiu QQ, Ducheyne P, Ayyaswamy PS. 3D Bone tissue engineered with bioactive microspheres in simulated microgravity. In Vitro Cellular & Developmental Biology-Animal. 2001; 37(3):157–165. [PubMed: 11370806]

Ravindran S, Roam JL, Nguyen PK, Hering TM, Elbert DL, McAlinden A. Changes of chondrocyte expression profiles in human MSC aggregates in the presence of PEG microspheres and TGF-beta 3. Biomaterials. 2011; 32(33):8436–8445. [PubMed: 21820171]

Ris F, Hammar E, Bosco D, Pilloud C, Maedler K, Donath MY, Oberholzer J, Zeender E, Morel P, Rouiller D, et al. Impact of integrin-matrix matching and inhibition of apoptosis on the survival of purified human beta-cells in vitro. Diabetologia. 2002; 45(6):841–850. [PubMed: 12107728]

Rogers GJ, Hodgkin MN, Squires PE. E-cadherin and cell adhesion: a role in architecture and function in the pancreatic islet. Cellular Physiology and Biochemistry. 2007; 20(6):987–994. [PubMed: 17982281]

Ruiz SA, Chen CS. Emergence of Patterned Stem Cell Differentiation Within Multicellular Structures. Stem Cells. 2008; 26(11):2921–2927. [PubMed: 18703661]

Samols E, Bonnerweir S, Weir GC. Intra-Islet Insulin Glucagon Somatostatin Relationships. Clinics in Endocrinology and Metabolism. 1986; 15(1):33–58. [PubMed: 2869846]

Schukur L, Zorlutuna P, Cha JM, Bae H, Khademhosseini A. Directed Differentiation of Size-Controlled Embryoid Bodies Towards Edothelial and Cardiac Lineages in RGD-Modified Poly(Ethylene Glycol) Hydrogels. Advanced Healthcare Materials. 2013; 2(1):195–205. [PubMed: 23193099]

Seeley, RR.; Stephens, TD.; Tate, P. Anatomy & Physiology. 5. McGraw-Hill; 2000. p. 1106

Silva AI, Mateus M. Development of a polysulfone hollow fiber vascular bio-artificial pancreas device for in vitro studies. Journal of Biotechnology. 2009; 139:236–249. [PubMed: 19121345]

Takei S, Teruya M, Grunewald A, Garcia R, Chan EK, Charles MA. Isolation and Function of Human and Pig Islets. Pancreas. 1994; 9(2):150–156. [PubMed: 8190716]

van Deijnen JHM, Hulstaert CE, Wolters GHJ, Vanschilfgaarde R. Significance of the Peri-Insular Extracellular Matrix for Islet Isolation from the Pancreas of Rat, Dog, Pig, and Man. Cell and Tissue Research. 1992; 267(1):139–146. [PubMed: 1735110]

Virtanen I, Banerjee M, Palgi J, Korsgren O, Lukinius A, Thornell LE, Kikkawa Y, Sekiguchi K, Hukkanen M, Konttinen YT, et al. Blood vessels of human islets of Langerhans are surrounded by a double basement membrane. Diabetologia. 2008; 51(7):1181–1191. [PubMed: 18438639]

Wang RN, Rosenberg L. Maintenance of beta-cell function and survival following islet isolation requires re-establishment of the islet-matrix relationship. Journal of Endocrinology. 1999; 163(2): 181–190. [PubMed: 10556766]

Weber LM, Anseth KS. Hydrogel encapsulation environments functionalized with extracellular matrix interactions increase islet insulin secretion. Matrix Biology. 2008; 27(8):667–673. [PubMed: 18773957]

Weber LM, Hayda KN, Anseth KS. Cell-Matrix Interactions Improve beta-Cell Survival and Insulin Secretion in Three-Dimensional Culture. Tissue Engineering Part A. 2008; 14(12):1959–1968. [PubMed: 18724831]

Weber LM, Hayda KN, Haskins K, Anseth KS. The effects of cell-matrix interactions on encapsulated beta-cell function within hydrogels functionalized with matrix-derived adhesive peptides. Biomaterials. 2007; 28(19):3004–3011. [PubMed: 17391752]

Yamada KM. Adhesive Recognition Sequences. Journal of Biological Chemistry. 1991; 266(20): 12809–12812. [PubMed: 2071570]

Zhu XH, Gan SK, Wang CH, Tong YW. Proteins combination on PHBV microsphere scaffold to regulate Hep3B cells activity and functionality: A model of liver tissue engineering system. Journal of Biomedical Materials Research Part A. 2007; 83A(3):606–616. [PubMed: 17503536]

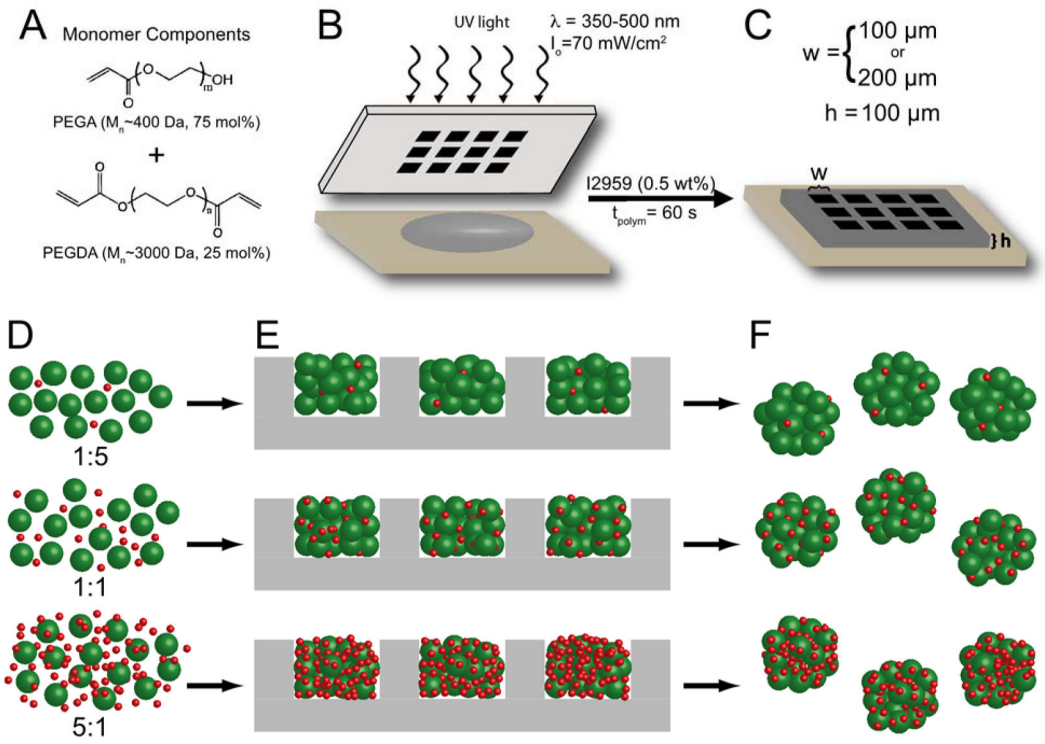

Figure 1. Formation of microwell arrays and cell-microparticle aggregates

(A) Monomer solution was created from a 15 wt% macromer solution of PEGA (M_n~400 Da) and PEGDA (M_n~3000 Da) in the molar ratios shown combined with photoinitiator I2959. (B) Hydrogel microwell arrays were formed via contact photolithography. Unpolymerized macromer solution (gray) was pipetted between an acrylated glass slide and a chrome photomask. The macromer solution was then polymerized through the photomask to create hydrogel microwell arrays (C). Microwell arrays were formed with well widths (w) of either 100 μm or 200 μm and well depths (h) of 100 μm. (D–F) Cell-microparticle aggregates were formed by (D) incubating MIN6 β-cells (green) with protein-laden particles (red) overnight to facilitate cell-protein interactions and promote a more uniform distribution. (E) Cell and microparticles were then seeded into hydrogel microwell arrays (gray) using centrifugation and orbital shaking. (F) After 5 days of static culture, cell-microparticle aggregates were removed from the microwell devices for imaging. Image not to scale.

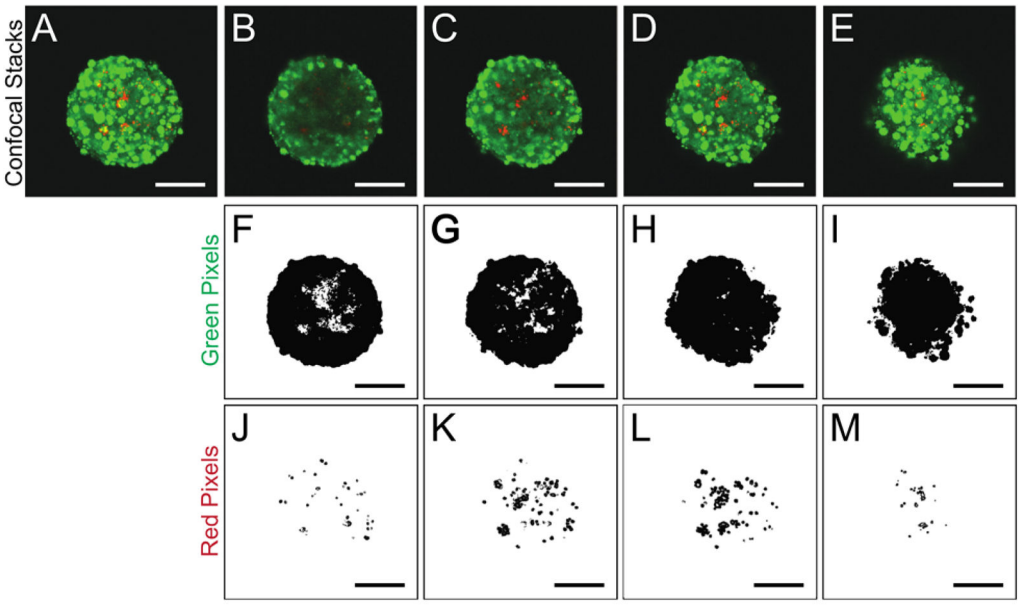

Figure 2. Determination of spatial distribution of microparticles

(A–E) Z-Projections of confocal images of cell-microparticle aggregates. MIN6 β-cells are stained with a CellTracker dye and appear green while laminin-coated microparticles appear red. (A) Entire cell-microparticle aggregate (~100 μm). (B–E) Smaller z-projection stacks taken throughout the z-dimension of the cell-microparticle aggregates starting at the bottom (B) and progressing upward to the top of the aggregate (E). (F–I) Green pixels (cells) in each stack. (J–M) Red pixels (microparticles) imaged in each corresponding stack. The red and green pixels detected in J–M and F–I, respectively, are used to determine total microparticle incorporation and spatial distribution of the microparticles throughout the z-direction. Scale bars represent 50 μm. Note: For image analysis done, a total of 10 z-projection stacks, each representing 10 μm, were analyzed for each aggregate. Four example stacks are shown here for clarity.

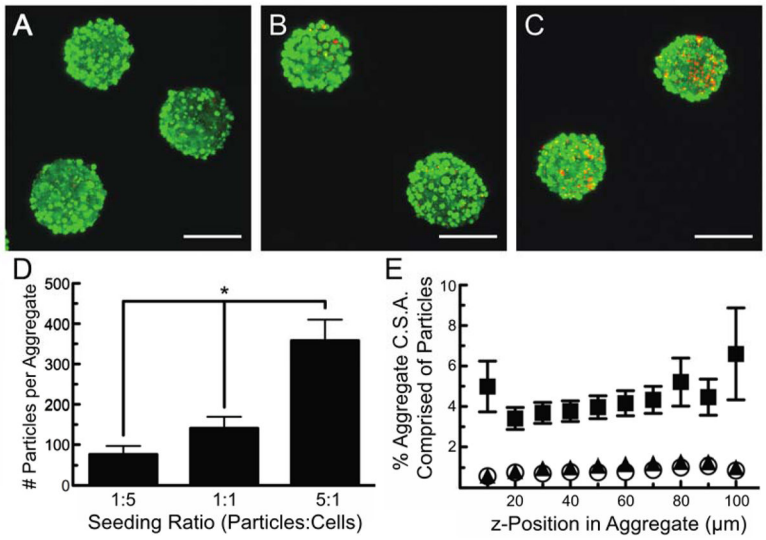

Figure 3. Microparticle incorporation within β-cell aggregates varies with seeding density

(A–C) Confocal images of cell-microparticle aggregates of MIN6 β-cells (green) and laminin-coated resin microparticles (red) seeded at ratios of (A) one particle for every five cells (1:5), (B) one particle for every cell (1:1), and (C) 5 particles for every cell (5:1). Scale bars represent 100 μm. (D) The total number of microparticles incorporated per aggregate as a function of seeding density. * indicates $p<0.05$ using one-way ANOVA. (E) Percentage of the cell-microparticle aggregate cross-sectional area comprised of microparticles at various z-positions within the aggregates seeded at microparticle:cell ratios of 1:5 (hollow circles), 1:1 (dark triangles), and 5:1 (dark squares). Error bars represent standard error of the mean for $n \geq 45$ aggregates.

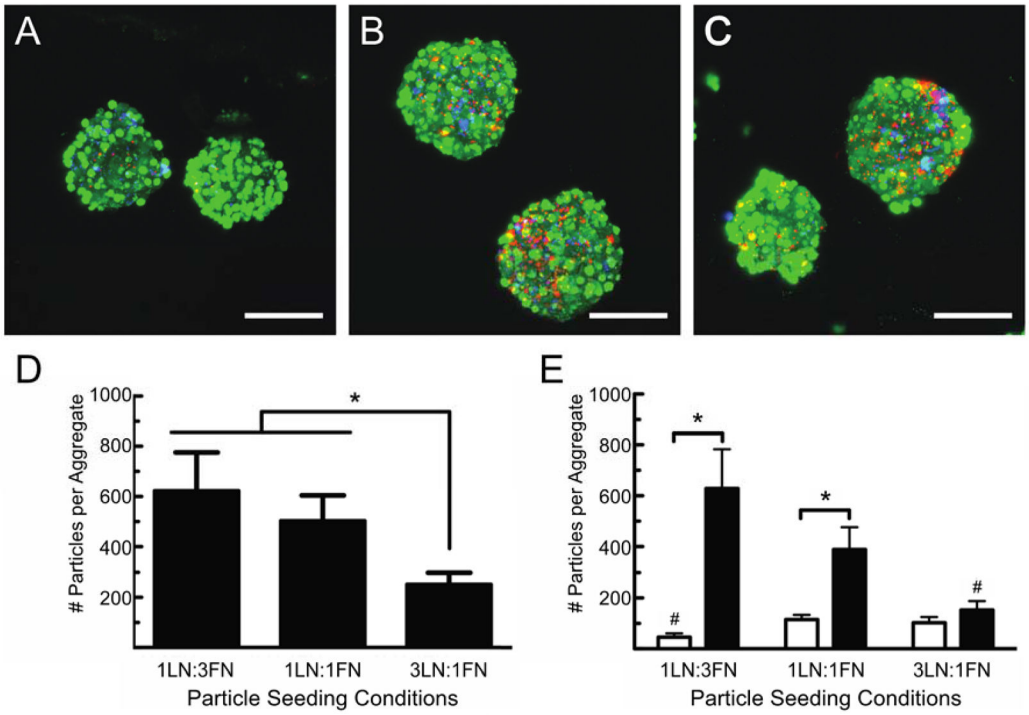

Figure 4. Two different ECM ligands are presented simultaneously to aggregated β-cells

(A–C) Confocal images of MIN6 β-cells (green) co-seeded with laminin-coated (red) and fibronectin-coated (blue) microparticles. The relative amount of each population of particle incubated with the MIN6 cells was varied prior to seeding at ratios of (A) 25% laminin coated microparticles and 75% fibronectin-coated microparticles (1LN:3FN), (B) 50% laminin-coated microparticles and 50% fibronectin-coated microparticles (1LN:1FN), and (C) 75% laminin-coated microparticles and 25% fibronectin-coated microparticles (3LN:1FN). Images are composite stacks of 50 images taken at 2 μm intervals and scale bars represent 100 μm. (D) Total number of particles, both laminin- and fibronectin-coated, incorporated per aggregate as a function of particle seeding condition. Significantly fewer particles are incorporated in the 3LN:1FN microparticle seeding condition ($p<0.05$ using one-way ANOVA). (E) Average number of microparticles from each population of incorporated per aggregate as a function of seeding conditions. White bars represent number of laminin-coated microparticles incorporated per aggregate and black bars represent number of fibronectin-coated microparticles per aggregate. $n \geq 25$ aggregates were measured for each seeding condition. * denotes significant difference between the number of particles of each kind incorporated for a given seeding condition, and # represents statistically significant number of particles incorporated compared to other seeding conditions for that type of particle. All statistical significances were determined using a $p<0.05$ and student's t-test.

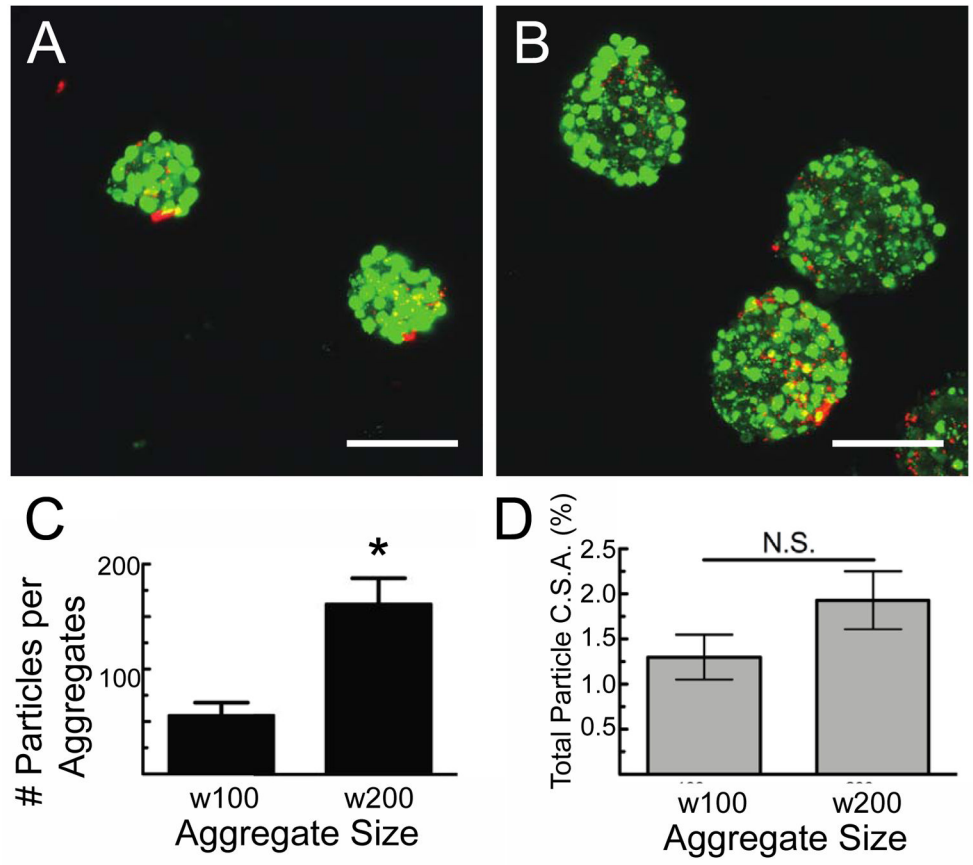

Figure 5. Effect of aggregate size on microparticle incorporation

Cell-microparticle aggregate size was controlled by incubation in different sized hydrogel microwell arrays. (A, B) Confocal images of MIN6 β-cells (green) and laminin-coated microparticles (red) formed in microwells with (A) 100 μm and (B) 200 μm. Scale bars represent 100 μm. (C) Quantification of the total number of microparticles incorporated per different size aggregates. * denotes $p<0.05$ using student's t-test. (D) Percent of the total cross-sectional area of each aggregate, summed over 100 μm in the z-direction, consisting of microparticles. No significant difference was found in the fraction of the aggregate occupied by microparticles relative to the percent occupied by cells. Error bars represent standard error of the mean for $n \geq 35$ aggregates measured of each size.

Table I

Protein present in cell-microparticle aggregates as a function of seeding conditions.

Cell: Microparticle Ratio	% LN Particles Seeded	% FN Particles Seeded	# LN Particles Incorporated	# FN Particles Incorporated	LN Presented (pg)	FN Presented (pg)
1:5	100%	---	80 ± 20	---	0.90	---
1:1	100%	---	140 ± 30	---	1.7	---
5:1	100%	---	360 ± 50	---	4.3	---
5:1	75%	25%	100 ± 20	150 ± 30	1.2	1.1
5:1	50%	50%	110 ± 20	390 ± 80	1.4	2.8
5:1	25%	75%	50 ± 10	580 ± 140	0.55	4.2